Post-print of: M. Meller and K. Stawiarski, "Capon-like DoA estimator for rotating arrays," 2019 International Radar Conference (RADAR), TOULON, France, 2019, pp. 1-6, doi: 10.1109/RADAR41533.2019.171281.

Capon-like DoA estimator for rotating arrays

Michał Meller*,† and Kamil Stawiarski†,*
* Gdańsk University of Technology, Faculty of Electronics, Telecommunications and Computer Science, Department of Automatic Control, ul. Narutowicza 11/12, 80-233 Gdańsk, POLAND
† PIT-RADWAR S.A., ul. Poligonowa 30, 04-051 Warsaw, POLAND
Corresponding author e-mail: michal.meller@eti.pg.edu.pl

***Abstract*—We propose a nonparametric superresolution DoA estimator that is suitable for use with rotating arrays. The proposed method can be regarded as an extension of the Capon approach. We investigate its properties using computer simulations and present results obtained by processing of real-world data.**

***Index Terms*—array processing, DoA estimation, azimuth estimation, Capon method, superresolution**

I. Introduction

Modern rotating arrays are a cost-effective solution of the 360 degree coverage requirement. Unlike systems that use stationary (non-rotating) arrays, which typically require three to four arrays facing different directions, the systems with rotating arrays can employ only one, which reduces the unit cost considerably. Moreover, the combination of mechanical and electronic scanning avoids many drawbacks of the purely-mechanical solution, although some limitations remain.

One of the difficulties that come with a rotating array is estimating the azimuth of the observed sources precisely. Systems with stationary antennas can take advantage of numerous superresolution methods, such as Capon [1], MUSIC [2] or ESPRIT [3], among others. The formulation of superresolution methods often involves estimating the signal covariance matrix, which means that an implicit assumption of signal stationarity takes place. Unfortunately, when the array rotates, this assumption does not hold, which limits the range of available techniques considerably.

In many systems, particularly legacy ones, the azimuth is estimated by a very simple algorithm that involves weighting of the array azimuth using the magnitude of the sum signal [4]. Another approach involves the averaging of the monopulse estimates [5], [6], but this method often fails at low signal to noise ratio. More recently, a family of parametric estimators based on the maximum likelihood principle was proposed [6], [7]. These estimators can offer very good accuracy provided that the number of sources included in the model is correct. However, their computational complexity grows substantially when the number of sources included in the model increases.

In this paper, we investigate the application of the nonparametric approach to the azimuth estimation problem. We propose a novel solution that one can regard as an extension of the Capon method. Using computer simulations, we investigate its properties when there are multiple, closely spaced, sources present and demonstrate that it has the superresolution property. We also include results obtained by processing of real-world data.

The paper adopts the following organization. Section II presents the formulation of the problem. In Section III, the proposed method is derived. Section IV reports results of computer simulations, while Section V presents real-world results. Finally, Section VI concludes the paper.

II. Problem statement

Denote by K the number of sources, and let ϕ_k, $k = 1, 2, \ldots, K$ denote the azimuth coordinate of k-th source. Suppose that N, M-variate complex vector valued, observations are available, $\mathbf{y}_n$, $n = 1, 2, \ldots, N$, and let $\phi_{\mathrm{a},n}$ denote the azimuth of the array at n-th observation.

Assuming that the source DoAs can be regarded as constant in the observation interval, one can model the observations as originating from

$$\mathbf{y}_n = \sum_{k=1}^{K} s_{k,n}\mathbf{a}(\Delta_n(\phi_k)) + \mathbf{v}_n \quad n = 1, 2, \ldots, N\,, \qquad (1)$$

where $s_{k,n}$ is the complex amplitude of k-th source at time n,

$$\Delta_n(\phi_k) = \phi_k - \phi_{\mathrm{a},n}$$

is the displacement of k-th source from the array boresight at time n, and $\mathbf{a}(\Delta\phi)$ denotes the array manifold, i.e., a mapping between the displacement of the source from the boresight $\Delta\phi$ and the corresponding array steering vector. Finally, $\mathbf{v}_n$ denotes the M-variate complex vector that represents noise and interference.

We will model the sources as zero-mean and mututally independent (noncorrelated) from each other and noise

$$\begin{aligned} \mathrm{E}[s_{k,n}] &= 0 \\ \mathrm{E}[s_{k_1,n_1}s^*_{k_2,n_2}] &= \sigma^2_{k_1}\delta(k_1 - k_2)\delta(n_1 - n_2) \\ \mathrm{E}[s_{k,n_1}v(n_2)] &= \mathbf{0}\,, \end{aligned}$$

where $\delta(\cdot)$ denotes the Kronecker delta function, z^* denotes the complex conjugate of z, and σ^2_k, $k = 1, 2, \ldots, K$ is the variance of k-th source, assumed to be an unknown deterministic quantity. Similarly, we will treat the covariance matrix of the noise and interference vector $\mathbf{v}_n$ as unknown and, due to the rotation of the array, possibly time-varying.

The quantities of interest, that is, the quantities that we wish to estimate, are the source angles ϕ_k, and the source variances σ_k^2, $1, 2, \ldots, K$. We will present the proposed solution of this problem in the next section.

III. Derivation of Capon-like estimator

We propose to estimate the source DoAs and variances using a novel nonparametric estimator, whose underlying principle is related to the classical Capon approach [1]. We will therefore succinctly discuss the latter method first.

A. Stationary array case – classical Capon estimator

For the stationary array case, without any loss of generality one may set $\phi_{\mathrm{a},n} = \phi_{\mathrm{a}} = 0$, which results in $\mathbf{a}(\Delta\phi) = \mathbf{a}(\phi)$. Additionally, it is typical to assume that the steering vectors are normalized, $\|\mathbf{a}(\Delta\phi)\| = 1$. The Capon method is obtained using the following argument. One can estimate the power originating from a direction ϕ using a beamformer

$$\hat{\sigma}^2(\phi) = \frac{1}{N}\sum_{n=1}^{N} |\mathbf{w}^{\mathrm{H}}(\phi)\mathbf{y}_n|^2 = \mathbf{w}^{\mathrm{H}}(\phi)\mathbf{R}_{\mathbf{y}}\mathbf{w}(\phi) \ , \quad (2)$$

where $\mathbf{w}(\phi)$ denotes the beamformer weight vector that must satisfy the distortionless constrant in the direction of interest

$$\mathbf{w}^{\mathrm{H}}(\phi)\mathbf{a}(\phi) = 1 \ , \quad (3)$$

and

$$\mathbf{R}_{\mathbf{y}} = \frac{1}{N}\sum_{n=1}^{N} \mathbf{y}_n\mathbf{y}_n^{\mathrm{H}}$$

is the correlation matrix of available observations.

To minimize the bias of $\hat{\sigma}^2(\phi)$, caused by the presence of multiple sources [leakage of spurious energy through sidelobes of the beampattern resulting from weight vector $\mathbf{w}(\phi)$], one can employ the adaptive beamforming approach. Specifically, the beamformer can be adapted to minimize $\hat{\sigma}^2(\phi)$ subject to (3)

$$\mathbf{w}(\phi) = \arg\min_{\mathbf{w}} \ \mathbf{w}^{\mathrm{H}}\mathbf{R}_{\mathbf{y}}\mathbf{w} \qquad \text{s.t.} \qquad \mathbf{w}^{\mathrm{H}}\mathbf{a}(\phi) = 1 \ . \quad (4)$$

The optimal weight vector takes the form

$$\mathbf{w}(\phi) = \frac{\mathbf{R}_{\mathbf{y}}^{-1}\mathbf{a}(\phi)}{\mathbf{a}^{\mathrm{H}}(\phi)\mathbf{R}_{\mathbf{y}}^{-1}\mathbf{a}(\phi)} \ ,$$

which, after substituting into (2), leads to the celebrated Capon method formula

$$\hat{\sigma}^2(\phi) = \frac{1}{\mathbf{a}^{\mathrm{H}}(\phi)\mathbf{R}_{\mathbf{y}}^{-1}\mathbf{a}(\phi)} \ . \quad (5)$$

The DoAs of the sources are found by localizing K highest peaks of (5).

B. Rotating-array case – Capon-like estimator

The classical Capon method employs the assumption that the sequence $\{\mathbf{y}_n\}$, $n = 1, 2, \ldots, N$ is wide-sense stationary. For a rotating array, this assumption does not hold because the source steering vectors $\mathbf{a}(\Delta_n(\phi_k))$ change with n. As a consequence, the estimator (5) will perform poorly in this situation. In this subsection, we will show how one can extend the the method to cope with this difficulty.

Assume that one can represent $\mathbf{a}(\Delta\phi)$ as a polynomial of a function $f(\Delta\phi)$

$$\mathbf{a}(\Delta\phi) = \sum_{p=0}^{P-1} \boldsymbol{\alpha}_p f^p(\Delta\phi) \ , \quad (6)$$

where $\boldsymbol{\alpha}_p$, $p = 0, 1, \ldots, P-1$ denote the complex vector coefficients, and $f^p(\Delta\phi) = [f(\Delta\phi)]^p$ denotes the p-th power of $f(\Delta\phi)$. Typical choices of $f(\Delta\phi)$ include, among others, the identity function

$$f(\Delta\phi) = \Delta\phi \ , \quad (7)$$

and the complex exponent

$$f(\Delta\phi) = e^{jc\sin(\Delta\phi)} \ , \quad (8)$$

where $c \neq 0$ is an arbitrary coefficient.

One can estimate the power originating from the direction ϕ using a time-varying beamformer

$$\hat{\sigma}^2(\phi) = \frac{\sum_{n=1}^{N} |\mathbf{w}_n^{\mathrm{H}}(\phi)\mathbf{y}_n|^2}{\sum_{n=1}^{N} \|\mathbf{a}(\Delta_n(\phi))\|^4} \ , \quad (9)$$

where $\mathbf{w}_n$ denotes the time-varying beamformer weight vector that satisfies

$$\mathbf{w}_n^{\mathrm{H}}(\phi)\mathbf{a}(\Delta_n(\phi)) = \|\mathbf{a}(\Delta_n(\phi))\|^2 \quad \forall_n \ . \quad (10)$$

We will construct the weight vector $\mathbf{w}_n(\phi)$ in the form analogous to used in eq. (6)

$$\mathbf{w}_n(\phi) = \mathbf{w}(\Delta_n(\phi)) = \sum_{q=0}^{Q-1} \boldsymbol{\omega}_p f^p(\Delta_n(\phi)) \ , \quad (11)$$

where $Q \geq P$, and adapt the coefficients $\boldsymbol{\omega}_q$, $q = 0, 1, \ldots, Q-1$, to minimize the sum that appears in the nominator of (9), i.e., to minimize $J = \sum_{n=1}^{N} |\mathbf{w}_n^{\mathrm{H}}(\phi)\mathbf{y}_n|^2$, subject to (10).

Substituting (11) into the objective yields

$$J = \sum_{n=1}^{N} |\mathbf{w}_n^{\mathrm{H}}(\phi)\mathbf{y}_n|^2 = \sum_{n=1}^{N} \left| \sum_{q=0}^{Q-1} \boldsymbol{\omega}_q^{\mathrm{H}} f^{*q}(\Delta_n\phi)\mathbf{y}_n \right|^2 = \sum_{q_1=0}^{Q-1}\sum_{q_2=0}^{Q-1} \boldsymbol{\omega}_{q_1}^{\mathrm{H}} \left[\sum_{n=1}^{N} f^{*q_1}(\Delta_n(\phi))\mathbf{y}_n\mathbf{y}_n^{\mathrm{H}} f^{q_2}(\Delta_n(\phi)) \right] \boldsymbol{\omega}_{q_2} \ . \quad (12)$$

Set

$$\mathbf{x} = \left[\boldsymbol{\omega}_0^{\mathrm{H}}\ \boldsymbol{\omega}_1^{\mathrm{H}}\ \ldots\ \boldsymbol{\omega}_{Q-1}^{\mathrm{H}}\right]^{\mathrm{H}}$$

$$\tilde{\mathbf{R}}_{\mathbf{y}} = \begin{bmatrix} \tilde{\mathbf{R}}_{0,0} & \tilde{\mathbf{R}}_{0,1} & \ldots & \tilde{\mathbf{R}}_{0,Q-1} \\ \tilde{\mathbf{R}}_{1,0} & \tilde{\mathbf{R}}_{1,1} & \ldots & \tilde{\mathbf{R}}_{1,Q-1} \\ \vdots & \vdots & \ddots & \vdots \\ \tilde{\mathbf{R}}_{Q-1,0} & \tilde{\mathbf{R}}_{Q-1,1} & \ldots & \tilde{\mathbf{R}}_{Q-1,Q-1} \end{bmatrix}, \quad (13)$$

where

$$\tilde{\mathbf{R}}_{q_1,q_2} = \sum_{n=1}^{N} f^{*q_1}(\Delta_n(\phi))\mathbf{y}_n\mathbf{y}_n^{\mathrm{H}} f^{q_2}(\Delta_n(\phi)) .$$

Using this notation, one may express the objective function as the following quadratic form

$$J = \mathbf{x}^{\mathrm{H}}\tilde{\mathbf{R}}_{\mathbf{y}}\mathbf{x} . \quad (14)$$

In the same way, one can rewrite eq. (10) as a linear constraint

$$\mathbf{A}\mathbf{x} = \mathbf{b} . \quad (15)$$

However, the exact forms of $\mathbf{A}$ and $\mathbf{b}$ depend on how $f(\Delta\phi)$ reacts to the complex conjugation, and each case requires careful evaluation. We discuss our illustrative examples (7), (8) separately.

Real-valued f: For $f(\Delta\phi)$ such as (7), where $f^*(\Delta\phi) = f(\Delta\phi)$, combining (6), (7), (10), and (11) leads to

$$\sum_{r=0}^{P+Q-2} \sum_{p+q=r} \boldsymbol{\alpha}_p^{\mathrm{H}}\boldsymbol{\omega}_q f^r(\Delta_n(\phi)) = \sum_{r=0}^{2P-2} \sum_{p_1+p_2=r} \boldsymbol{\alpha}_{p_1}^{\mathrm{H}}\boldsymbol{\alpha}_{p_2} f^r(\Delta_n(\phi)) , \quad (16)$$

which must hold for $n = 1, 2, \ldots, N$. For sufficiently large values of N, the two polynomials of $f(\Delta\phi)$ that appear on the left and the right side of the above equation are equal to each other only when their coefficients are equal, i.e., when

$$\sum_{p+q=r} \boldsymbol{\alpha}_p^{\mathrm{H}}\boldsymbol{\omega}_q = \begin{cases} b_r & \text{for} \quad r = 0, 1, \ldots, 2P-2 \\ 0 & \text{for} \quad r = 2P-1, \ldots, P+Q-2 \end{cases},$$

where

$$b_r = \sum_{p_1+p_2=r} \boldsymbol{\alpha}_{p_1}^{\mathrm{H}}\boldsymbol{\alpha}_{p_2} .$$

Using $\mathbf{x}$ defined in eq. (13), one can summarize the above system of equations in the matrix form (15), where $\mathbf{A}$ is a $(P+Q-1) \times MQ$ matrix of the form

$$\mathbf{A} = \begin{bmatrix} \boldsymbol{\alpha}_0^{\mathrm{H}} & \mathbf{0} & \mathbf{0} & \ldots & \mathbf{0} \\ \boldsymbol{\alpha}_1^{\mathrm{H}} & \boldsymbol{\alpha}_0^{\mathrm{H}} & \mathbf{0} & \ldots & \mathbf{0} \\ \boldsymbol{\alpha}_2^{\mathrm{H}} & \boldsymbol{\alpha}_1^{\mathrm{H}} & \boldsymbol{\alpha}_0^{\mathrm{H}} & \ldots & \mathbf{0} \\ \vdots & \ddots & \ddots & \ddots & \vdots \\ \boldsymbol{\alpha}_{P-1}^{\mathrm{H}} & \boldsymbol{\alpha}_{P-2}^{\mathrm{H}} & \boldsymbol{\alpha}_{P-3}^{\mathrm{H}} & \ddots & \vdots \\ \mathbf{0} & \boldsymbol{\alpha}_{P-1}^{\mathrm{H}} & \boldsymbol{\alpha}_{P-2}^{\mathrm{H}} & \ddots & \vdots \\ \vdots & \ddots & \ddots & \ddots & \vdots \\ \mathbf{0} & \mathbf{0} & \ldots & \mathbf{0} & \boldsymbol{\alpha}_{P-1}^{\mathrm{H}} \end{bmatrix}$$

and $\mathbf{b}$ is a $P+Q-1$ element vector defined below

$$\mathbf{b} = \begin{bmatrix} b_0 & b_1 & \ldots & b_{2P-2} & 0 & \ldots & 0 \end{bmatrix}^{\mathrm{T}} .$$

Complex-valued f: For f in the form given by eq. (8), it holds that $f^*(\Delta\phi) = f^{-1}(\Delta\phi)$. The combination of (6), (8), (10), and (11) results in

$$\sum_{r=-Q+1}^{P-1} \sum_{p-q=r} \boldsymbol{\omega}_q^{\mathrm{H}}\boldsymbol{\alpha}_p f^r(\Delta_n(\phi)) = \sum_{r=-P+1}^{P-1} \sum_{p_2-p_1=r} \boldsymbol{\alpha}_{p_1}^{\mathrm{H}}\boldsymbol{\alpha}_{p_2} f^r(\Delta_n(\phi)) , \quad (17)$$

which can be expressed as (15) with

$$\mathbf{A} = \begin{bmatrix} \mathbf{0} & \ldots & \mathbf{0} & \mathbf{0} & \boldsymbol{\alpha}_0^{\mathrm{H}} \\ \mathbf{0} & \ldots & \mathbf{0} & \boldsymbol{\alpha}_0^{\mathrm{H}} & \boldsymbol{\alpha}_1^{\mathrm{H}} \\ \mathbf{0} & \ldots & \boldsymbol{\alpha}_0^{\mathrm{H}} & \boldsymbol{\alpha}_1^{\mathrm{H}} & \boldsymbol{\alpha}_2^{\mathrm{H}} \\ \vdots & \iddots & \iddots & \iddots & \vdots \\ \boldsymbol{\alpha}_{P-2}^{\mathrm{H}} & \boldsymbol{\alpha}_{P-1}^{\mathrm{H}} & \mathbf{0} & \ldots & \mathbf{0} \\ \boldsymbol{\alpha}_{P-1}^{\mathrm{H}} & \mathbf{0} & \mathbf{0} & \ldots & \mathbf{0} \end{bmatrix}$$

and

$$\mathbf{b} = \begin{bmatrix} 0 & \ldots & 0 & b_{-P+1} & \ldots & b_0 & \ldots & b_{P-1} \end{bmatrix}^{\mathrm{T}}$$

with

$$b_r = \sum_{p_2-p_1=r} \boldsymbol{\alpha}_{p_1}^{\mathrm{H}}\boldsymbol{\alpha}_{p_2} .$$

Again, the dimensions of $\mathbf{A}$ and $\mathbf{b}$ are $(P+Q-1) \times MQ$, and $P+Q-1 \times 1$, respectively.

Discussion: The solution of the optimization problem stated in equations (14), (15) exists provided that the matrix $\tilde{\mathbf{R}}_{\mathbf{y}}$ is nonsingular, in which case it reads

$$\mathbf{x} = \tilde{\mathbf{R}}_{\mathbf{y}}^{-1}\mathbf{A}^{\mathrm{H}}\left[\mathbf{A}\tilde{\mathbf{R}}_{\mathbf{y}}^{-1}\mathbf{A}^{\mathrm{H}}\right]^{-1}\mathbf{b} . \quad (18)$$

The smallest number of observations required for $\tilde{\mathbf{R}}_{\mathbf{y}}$ to be invertible is MQ, which is a straightforward consequence of the observation that

$$\tilde{\mathbf{R}}_{\mathbf{y}} = \mathbf{D}\mathbf{D}^{\mathrm{H}} ,$$

where

$$\mathbf{D} = \begin{bmatrix} \mathbf{y}_1 f^{*0}(\Delta_1(\phi)) & \ldots & \mathbf{y}_N f^{*0}(\Delta_N(\phi)) \\ \mathbf{y}_1 f^{*1}(\Delta_1(\phi)) & \ldots & \mathbf{y}_N f^{*1}(\Delta_N(\phi)) \\ \vdots & \ddots & \vdots \\ \mathbf{y}_1 f^{*Q-1}(\Delta_1(\phi)) & \ldots & \mathbf{y}_N f^{*Q-1}(\Delta_N(\phi)) \end{bmatrix} .$$

Finally, observe that, despite the large dimension of the vector $\mathbf{x}$, which equals MQ, the actual number of degrees of freedom can be considerably smaller. Since there are $P+Q-1$ constraints, there problem has $MQ-P-Q+1 = (M-1)Q-P+1$ degrees of freedom, which also means that $M \geq 2$ is required to make the optimization problem feasible.

IV. Simulation results

One may investigate the behavior of the proposed estimator using the computer simulation approach. In our case, we modeled a system with the standard (half-wavelength element spacing) uniform linear array with $M = 4$ elements. Due to the small size of the array, its classical limit of resolution is 30°. We simulated the rotation of the array between 0° and 12.7°, and took measurements every 0.1°, which results in $N = 128$ observations.

We compared the behavior of the baseline, nonadaptive estimator,

$$\hat{\sigma}^2(\phi) = \frac{\sum_{n=1}^{N} |\mathbf{a}_n^{\mathrm{H}}(\Delta_n\phi)\mathbf{y}_n|^2}{\sum_{n=1}^{N} \|\mathbf{a}(\Delta_n(\phi))\|^4} , \tag{19}$$

and the proposed Capon-like approach. In the case of the latter, we described the array manifold using (6) with $P = M = 4$,

$$f(\Delta\phi) = e^{j\pi \sin(\Delta\phi)} ,$$

and

$$\boldsymbol{\alpha}_0 = \mathbf{e}_1 \qquad \boldsymbol{\alpha}_1 = \mathbf{e}_2 \qquad \boldsymbol{\alpha}_2 = \mathbf{e}_3 \qquad \boldsymbol{\alpha}_3 = \mathbf{e}_4 ,$$

where $\mathbf{e}_i$ denotes the vector than consists of zeros except one at the i-th element. To construct the time-varying adaptive beamformer, we used $Q = 6$. Moreover, to avoid possible problems with ill-conditioning of the matrix $\tilde{\mathbf{R}}_{\mathbf{y}}$, we employed the diagonal loading technique, i.e., we added the identity matrix to the product $\mathbf{D}\mathbf{D}^{\mathrm{H}}$.

Fig. 1 shows a comparison of typical aziumuth spectra obtained using the two solutions for a single source, placed at 10°. Using the proposed approach, tho source, whose SNR was equal to 20 dB, was localized properly. Moreover, the shape of the spectra clearly suggests that the proposed estimator has the superresolution property known from the classical Capon method.

One may confirm this observation easily by simulating an additional source. Fig. 2 shows the angular spectra for two sources 20 dB above noise, placed at 5° and 20°. The nonadaptive estimator fails to resolve the sources, while the proposed one can separate them. We verified that, in this scenario, the method can resolve the sources separated by 9°.

Finally, we compared accuracy of the proposed method with the classical Capon approach, implemented by neglecting the fact that the antenna rotates. To this end, we treated the rotating antenna as if it was stopped is in the middle of the angular sector covered by the N observations, i.e., at 6.4°, and proceeded with (5). Fig. 3 shows the comparison of typical angular spectral estimates obtained using the proposed method and the classical approach in the single-source and the two-source scenarios. It is clear that the proposed approach is the superior one, as it exhibits better resolution.

Ta evaluate the performance of the proposed method in relative and absolute terms, we compared its accuracy with the Crámer-Rao lower bound (CRB), the maximum likelihood approach, and the classical method, implemented as above.

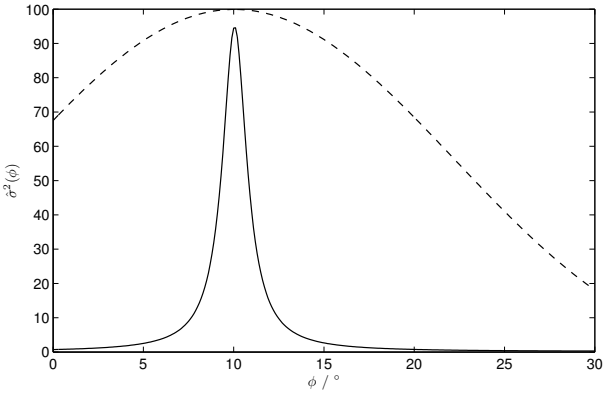

Figure 1. Comparison of typical angular spectral estimates obtained using a nonadaptive beamformer (dashed line) and the proposed method (solid line) for a single source at 10°.

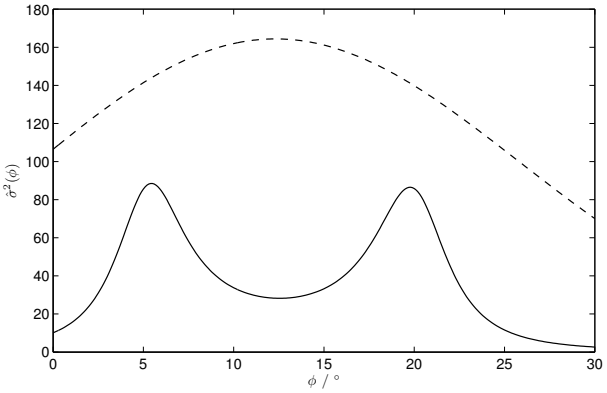

Figure 2. Comparison of typical angular spectral estimates obtained using a nonadaptive beamformer (dashed line) and the proposed method (solid line) for two sources at 5° and 20°, respectively.

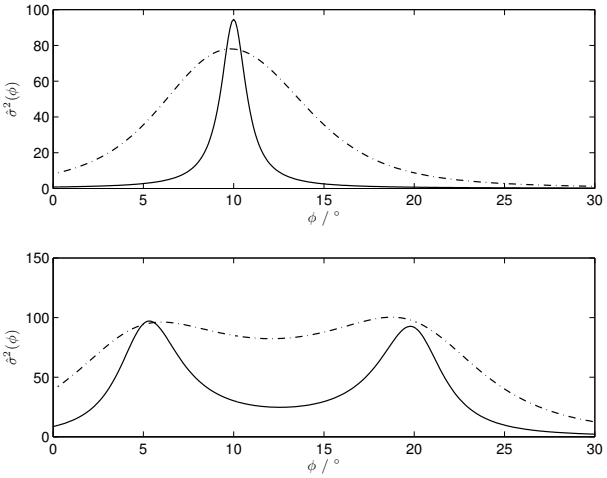

Figure 3. Comparison of typical angular spectral estimates obtained using the proposed method (solid line) and the classical one (dashed line) for the single-source (top plot) and the two-source scenario (bottom plot).

Both the maximum likelihood estimator and the CRB were based on the assumptions presented in Section II with the number of sources $K = 1$ – the corresponding form of the log-likelihood function reads

$$l(\phi_1, \sigma_1^2, \sigma_v^2) = \\ C - \left[\sum_{n=1}^{N} \log\det \mathbf{R}_n(\phi_1, \sigma_1^2, \sigma_v^2) + \mathbf{y}_n^{\mathrm{H}} \mathbf{R}_n^{-1}(\phi_k, \sigma_1^2, \sigma_v^2) \mathbf{y}_n \right], \tag{20}$$

where C is a constant, whose exact form is of little importance to the maximum likelihood estimator, and

$$\mathbf{R}_n(\phi_1, \sigma_1^2, \sigma_v^2) = \sigma_v^2 \boldsymbol{I} + \sigma_1^2 \mathbf{a}(\Delta_n(\phi_1)) \mathbf{a}^{\mathrm{H}}(\Delta_n(\phi_1))$$

is the covariance matrix of n-th observation. The maximization of the log-likelihood was performed using a fast approximate method proposed in [5]. In this method, the optimal values of the parameters σ_v^2 and σ_1^2 are approximated by projecting the data on the noise and the signal subspaces, and inserted into (20). The corresponding formulas read

$$\hat{\sigma}_v^2(\phi_1) = \frac{1}{N} \sum_{n=1}^{N} \mathbf{y}_n^{\mathrm{H}} \mathbf{Q}_n(\phi_1) \mathbf{y}_n$$

$$\hat{\sigma}_1^2(\phi_1) = \frac{\sum_{n=1}^{N} \mathbf{y}_n^{\mathrm{H}} \mathbf{P}_n(\phi_1) \mathbf{y}_n - N \hat{\sigma}_v^2(\phi_1)}{\sum_{n=1}^{N} \mathbf{a}^{\mathrm{H}}(\Delta_n(\phi_1)) \mathbf{a}(\Delta_n(\phi_1))}$$

where

$$\mathbf{Q}_n(\phi_1) = \boldsymbol{I} - \frac{\mathbf{a}(\Delta_n(\phi_1)) \mathbf{a}^{\mathrm{H}}(\Delta_n(\phi_1))}{\mathbf{a}^{\mathrm{H}}(\Delta_n(\phi_1)) \mathbf{a}(\Delta_n(\phi_1))}$$

$$\mathbf{P}_n(\phi_1) = \frac{\mathbf{a}(\Delta_n(\phi_1)) \mathbf{a}^{\mathrm{H}}(\Delta_n(\phi_1))}{\mathbf{a}^{\mathrm{H}}(\Delta_n(\phi_1)) \mathbf{a}(\Delta_n(\phi_1))}$$

are the noise and the signal subspace projection matrices, respectively.

Such an approach reduces the number of arguments in the log-likelihood from three to one, which improves its convergence speed greatly. Despite this simplification, the resultant accuracy of the angle estimates seems to not degrade significantly from the practical point of view.

Fig. 4 shows the results of such a comparison performed for a source at $\phi_1 = 5^\circ$ and $M = P = Q = 4$. To evaluate the estimators' MSE, we performed 2500 Monte Carlo simulations for each value of SNR. Not unexpectedly, the classical method is the least accurate, and its performance drops at high SNRs, where the bias caused by neglecting the array rotation starts to dominate. The proposed approach and the maximum likelihood method behave much better, and reach the CRB for higher values of SNR. Remarkably, the proposed approach behaves slightly better in the threshold area, i.e., for SNR around -7 dB, which is where the accuracy of the estimators starts to break down. The somewhat poorer behavior of the maximum likelihood estimator is likely related to the application of the approximate minimization method described above.

To investigate possible adverse effects of increasing Q, we repeated the above experiment with Q, equal to 6 and 8. There

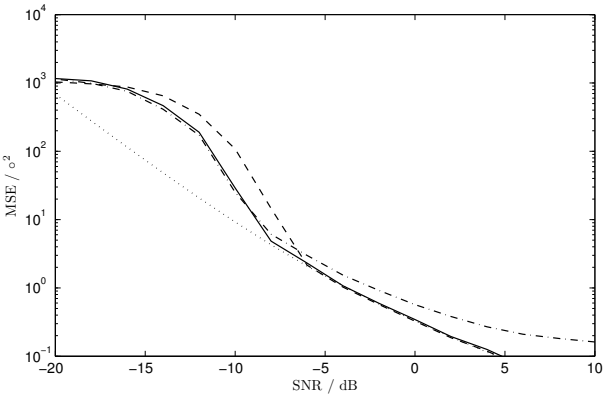

Figure 4. Dependence of the proposed method's mean-square error on the source signal to noise ratio (solid line), compared with the maximum likelihood approach (dashed line), classical Capon estimator (dash-dotted line), and the corresponding Crámer-Rao lower bound (dotted line). The simulations were performed for the standard uniform linear array with $M = 4$ elements, and $N = 128$, $P = 4$, $Q = 4$.

difference in the observed behavior of the proposed estimator were negligible, although the computation time increased considerably.

V. Application to real-world data

We applied the proposed method to real-world data we used previously in [5]. The data consists of 689 sequences $\mathbf{y}_n$, $n = 1, 2, \ldots, N$, with $N = 1024$ obtained by observing a cooperative target. Unlike in Section IV, where we used the element-space processing, in this dataset the radar array output was preprocessed using a beamformer, so that each observation vector $\mathbf{y}_n$ has only two elements that correspond to the sum and the difference beam of the radar. Typical contents of the dataset are shown shown in Fig. 5.

The adopted representation of the array manifold $\mathbf{a}(\Delta\phi)$ employs $P = 6$ components and the following form of $f(\Delta\phi)$

$$f(\Delta\phi) = \begin{cases} \Delta\phi & \text{for} \quad |\Delta\phi| \leq \Delta_{\max} \\ 0 & \text{for} \quad |\Delta\phi| > \Delta_{\max} \end{cases}$$

where $\Delta_{\max}$ equals $0.75\phi_{3dB}$, and ϕ_{3dB} is the 3-dB beamwidth of the sum beam. The clipping of $f(\Delta\phi)$ improves the behavior of the approximation in the sidelobe region of the sum and difference beampatterns, which would otherwise diverge for high values of $\Delta\phi$.

Fig. 6 compares the histograms of the azimuth estimation errors, normalized by the 3 dB beamwidth of the system, obtained using the ML estimator and the proposed method with $Q = P$. Both methods exhibit a small bias, equal to $0.013\phi_{3dB}$ for the ML estimator and $0.016\phi_{3dB}$ for the proposed method. We attribute the existence of the bias to inaccuracies in our model of the array manifold. Despite having smaller bias, the ML estimator actually has slightly larger RMS error – $0.049\phi_{3dB}$ – than the proposed method – $0.046\phi_{3dB}$. Overall, however, the differences are so small, that it seems fair to say that the accuracy of both methods is comparable. The proposed estimator, however, allows one to resolve multiple sources in

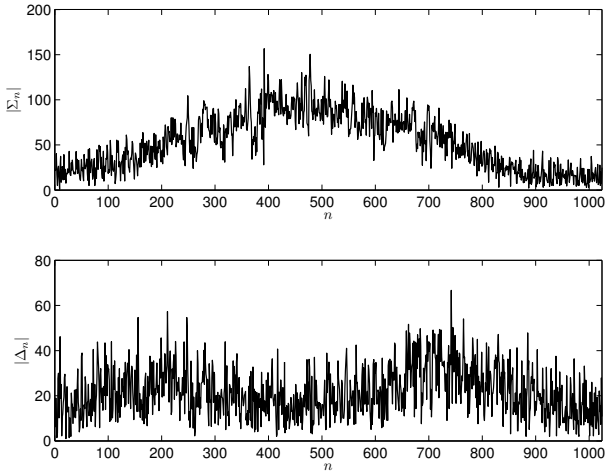

Figure 5. Typical realization of $\mathbf{y}_n$ for the case of real-world data: top plot – sum beam, bottom plot – difference beam.

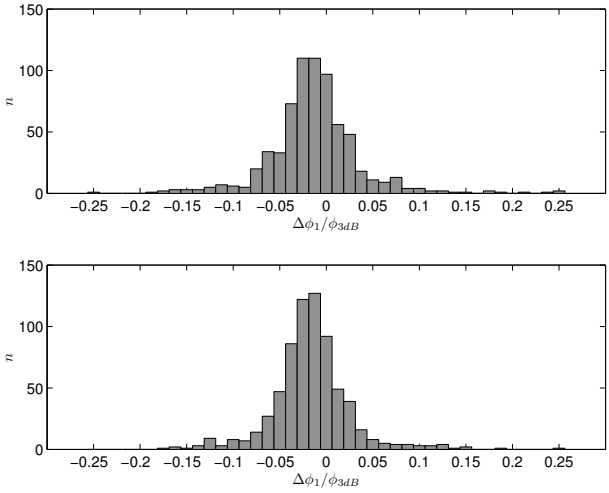

Figure 6. Comparison of histograms of azimuth estimation errors obtained using ML estimator and proposed method.

a more straightforward way. While in the case of the ML method one is required to increase the number of parameters in the model, which increases the computational complexity considerably, the proposed nonparametric approach simply requires one to scan the spectrum estimate (9) for the presence of multiple peaks.

VI. Conclusions

We proposed a Capon-like DoA estimator that is suitable for the application in systems with rotating-arrays. The method, which employs time-varying adaptive beamforming, can achieve sub-beamwidth resolution. Its properties were verified using several computer simulation experiments. Results obtained using real-world data were also presented.

References

[1] J. Capon, "High resolution frequency-wavenumber spectrum analysis," *Proceeding of the IEEE*, vol. 57, p. 1408–1418, 1969.

[2] R. Schimidt, "Multiple emiter location and signal parameter estimation," *IEEE Transactions on Antennas and Propagation*, vol. 34, no. 3, pp. 276–280, 1986.

[3] R. Roy and T. Kailath, "ESPRIT – Estimation of Signal Parameters via Rotational Invariance Techniques," *IEEE Transactions on Acoustics, Speech and Signal Processing*, vol. 37, no. 7, pp. 984–995, 1989.

[4] D. K. Barton, *Radar System Analysis and Modeling*. Artech House, Inc., 2005.

[5] M. Meller, K. Stawiarski, and B. Pikacz, "Azimuth estimator for a rotating array radar with wide beam," *Proc. SPIE*, vol. 10715, pp. 10 715 – 10 715 – 5, 2018. [Online]. Available: https://doi.org/10.1117/12.2317865

[6] M. Greco, F. Gini, and A. Farina, "Joint use of Σ and Δ channels for multiple radar target DOA estimation," in *Proc. 2005 13th European Signal Processing Conference (EUSIPCO 2005)*, 2005.

[7] A. Farina, F. Gini, and M. Greco, "DOA estimation by exploiting the amplitude modulation induced by antenna scanning," *IEEE Transactions on Aerospace and Electronic Systems*, vol. 38, no. 4, pp. 1276–1286, 2002.